ARTICLE

Effectiveness of observation-domain sidereal filtering for GPS precise point positioning

Christopher Atkins* and Marek Ziebart
Department of Civil, Environmental and Geomatic Engineering
University College London
Gower Street
London
*e-mail: ucescat@ucl.ac.uk, Tel/Fax: +44 (0) 20 7679 3638 / 7380 0986

Abstract
Sidereal filtering is a technique used to reduce errors caused by multipath in the positioning of static receivers via the Global Positioning System (GPS). It relies upon the receiver and its surrounding environment remaining static from one day to the next and takes advantage of the approximately sidereal repeat time of the GPS constellation geometry. The repeating multipath error can thus be identified, usually in the position domain, and largely removed from the following day. We describe an observation-domain sidereal filter algorithm that operates on undifferenced ionospheric-free GPS carrier phase measurements to reduce errors caused by multipath. It is applied in the context of high-rate (1 Hz) precise point positioning (PPP) of a static receiver. An observation-domain sidereal filter (ODSF) is able to account for the slightly different repeat times of each GPS satellite, unlike a position-domain sidereal filter (PDSF), and can hence be more effective at reducing high-frequency multipath error. Using eight-hour long datasets of GPS measurements from two different receivers with different antenna types and contrasting environments, the ODSF algorithm is shown overall to yield a position time series 5-10% more stable, in terms of Allan deviation, than a PDSF over nearly all time intervals below about 200 s in length. This may be particularly useful for earthquake and tsunami early warning systems where the accurate measurement of small displacements of the ground over the period of just a few minutes is crucial. However, the sidereal filters are also applied to a third dataset during which two short episodes of particularly high-frequency multipath error were identified. These two periods are analyzed in detail and illustrate the limitations of using sidereal filters with important implications for other methods of correcting for multipath at the observation level.

Introduction

Global Navigation Satellite Systems (GNSS) are used in earthquake monitoring and tsunami warning systems, e.g. the GPS Real Time Earthquake and Tsunami (GREAT) Alert System (www.gdgps.net/products/great-alert.html) and the Real-time Earthquake Analysis for Disaster Mitigation Network (READI) (www.sopac.ucsd.edu). For this application, GNSS carrier phase measurements are recorded at a static receiver antenna continuously at 1 Hz or above. However, the ability of GNSS to measure centimeter-level ground displacements is limited by several error sources, one of which is multipath interference. Multipath can introduce phase measurement errors at frequencies and amplitudes similar to seismic waves (Larson et al 2007). Such errors alias into position calculations and can be misinterpreted as seismic waves and vice versa. Also, a small centimeter-level permanent displacement of an antenna caused by the earthquake is more likely to be obscured by these errors.

Sidereal filtering, introduced by Bock (1991) and Genrich and Bock (1992), is a method for mitigating the effect of multipath interference on GPS carrier phase measurements at stationary receiver antennas. It takes advantage of the fact that GPS satellites have an orbital period of about 11 hours 58 minutes, completing two orbits for every rotation of the earth about its axis. For a static receiver, this means the geometry relating the receiver antenna, surrounding reflectors and satellites will repeat approximately every sidereal day. Hence, as multipath error is highly dependent on this geometry, then these errors should repeat every sidereal day. Assuming the antenna, its surrounding environment and the reflective properties of that environment remain static, the repeating multipath error pattern can hence be empirically derived and then removed, often in the position domain. Sidereal filtering can theoretically reduce any error source that repeats every sidereal day. Hence, particularly in precise applications, imperfections in antenna phase center models can also be mitigated.

Examples in the literature that apply sidereal filtering in the position (or coordinate) domain are Elósegui et al (2006) and Bilich et al (2008). These apply the technique in the positioning of a receiver antenna relative to at least one other static receiver, rather than precise point positioning (PPP), which is a technique to calculate the position of a receiver antenna to an accuracy of a few centimeters using a *single* receiver and precise satellite clock and orbit data (Zumberge et al 1997). Many apply the modified sidereal filtering (MSF) technique proposed by Choi et al (2004). Prior to this influential paper, the repeat period used for sidereal filtering was one sidereal day, 23 h 56 m 4 s (86,164 s). Choi et al (2004) pointed out that the repeat time varied for each GPS satellite and could be calculated using the GPS broadcast ephemeris and Kepler's Third Law. The average repeat time for the whole constellation is actually around 23 h 55 m 55 s (86,155 s). The reason for this is that it is an operational constraint for GPS that the ground track of each satellite is fixed. For this to be achieved, the orbital period is set to be roughly four seconds faster than a half-sidereal period. This compensates the westward drift of the longitude of

the ascending node caused by the earth's oblateness (Choi et al 2004). Since this period is no longer strictly sidereal, the name modified sidereal filtering (MSF) is used. The difference between these two 'sidereal' periods is only about nine seconds. However, for high-accuracy positioning using carrier phase measurements at high rates, say 1 Hz, an accurate repeat time is important because multipath error can change significantly over just a few seconds. The figure of 86,155 seconds is only an overall mean value of GPS ground track repeat periods (with outliers excluded). Each satellite has its own repeat period, usually within five seconds of this value. Occasional exceptions occur when satellites are maneuvered, causing the orbital period to differ from this nominal value by up to tens of seconds.

Another method of calculating a repeat period appears in Axelrad et al (2005): Considering one GPS satellite at a particular epoch, an epoch on the preceding day is found that most closely corresponds to the satellite occupying the same position in the sky in terms of azimuth and elevation in the receiver's local topocentric (east-north-up) coordinate system. Such a search is executed by maximizing the dot-product of the two receiver-satellite unit vectors. This repeat time may differ from the previous method, which used Kepler's Third Law, because of parallax (Agnew and Larson 2007), i.e. it should be more relevant for an observer on the earth's surface rather than a hypothetical observer at the center of the earth. This repeat time is named aspect repeat time (ART) by Agnew and Larson (2007). The 'constellation repeat time' is then calculated as the mean of all satellite repeat times. However, as the paper points out, it seems a shame to lose the advantages of accurately calculating the repeat time of each satellite only to combine them together to find a 'constellation repeat time' and apply multipath corrections in the position domain. One solution to this would be to apply the sidereal filter in the observation domain, i.e. measurement residuals from, say, the previous day are used to derive corrections to the measurements on the 'current' day. Lau (2012) and Ragheb et al (2007) found no significant difference between applying corrections for multipath error in the position domain and the observation domain, although these studies used double-differenced measurements (Leick et al 2015). Complications can arise. For example, all double-differenced measurements, and hence double-differenced measurement residuals, would each be associated with two satellites (and two receivers) and therefore two different ground-track repeat periods. Hence, to apply a rigorous sidereal filter to a series of double-differenced measurements, should the average of the two repeat times be used? Should the repeat time of the satellite at the lower elevation be used since that satellite is more likely to be affected by multipath? The answers to these questions are not obvious. Ragheb et al (2007), for example, determines the shift period required to produce the maximum correlation of the double-differenced measurement residuals from both days.

In PPP, this complication can be avoided because all measurements are usually undifferenced, although some studies, such as Geng et al (2013), employ PPP with single-differencing across satellites to remove receiver hardware delays and clock errors. Sidereal filtering has been applied in PPP scenarios, but these have largely taken place in the position domain, e.g. Takasu (2006), Shi (2012) and Hung and Rau (2013). Very few studies consider observation-domain sidereal filtering in PPP. One such example appears in Reuveni et al (2012), but is applied to GPS data

recorded at a rate of only once every thirty seconds in order to measure sub-daily seismic strain.

Sidereal filtering in the observation domain also offers advantages during satellite outages. For example, if an outage occurs on one satellite, corrections for multipath error should still be valid for all other visible satellites, whereas corrections applied in the position domain would not be valid. However, we do not assess this advantage here. Larson et al (2007) addressed this difficulty by pre-editing the input measurement files to ensure that the same satellites were visible each day.

One alternative to sidereal filtering would be to map PPP phase residuals onto a 'skyplot' consisting of 'cells' of a few degrees in elevation and azimuth as demonstrated in Granström (2006) and Fuhrmann et al (2014). The mean value of each cell could then used as a correction to satellite measurements within that cell. However, as will be seen in the analysis below, these cells are too large to capture the effects of high-frequency phase multipath errors. In this study, 'high-frequency multipath' refers to oscillatory multipath errors with periods under about 1,000 s.

We use a 'dot-product' algorithm (described below) derived from the 'aspect repeat time' method (Axelrad et al 2005; Agnew and Larson 2007) to calculate individual GPS satellite repeat times and apply it to observation-domain sidereal filtering of undifferenced ionospheric-free phase measurements in high-rate 1 Hz precise point positioning. The filter performance is compared with other observation-domain sidereal filter variants and a position-domain sidereal filter over two 8-hour datasets sourced from different receivers. The ability of the sidereal filters to remove high-frequency multipath error is then assessed by applying them to two example datasets spanning fifteen minutes each and using Allan deviation to measure stability of the resulting position time series.

Observation-domain sidereal filter (ODSF) algorithm
To best describe the observation-domain sidereal filter (ODSF) algorithm, a simple arbitrary example is used. Assume that two sets of GPS data, collected on adjacent days, are available: Day 1 and Day 2. The 'true' earth-centered earth-fixed (ECEF) position of the receiver on Day 1 is already known, either by processing Day 1 to yield an average position, or by some other method. The objective is to remove the effect of multipath interference from Day 2 by applying a sidereal filter. This filter will use information from Day 1 to compute the necessary multipath corrections.

For this study, only GPS ionospheric-free *phase* measurements, denoted Φ_{IF} (in units of meters), are used. These are formed by using a linear combination of GPS L1 and L2 phase measurements. However, measurement noise is increased threefold and phase multipath errors can become larger: if phase multipath theoretically cannot exceed a quarter of a wavelength (Misra and Enge 2001), i.e. 4.8 cm and 6.1 cm for the L1 and L2 carriers respectively, then multipath error for ionospheric-free phase observations can reach a theoretical maximum of 21.5 cm. In practice, phase multipath errors of this magnitude are unlikely, but phase multipath does indeed become more significant. Code measurements are not used in the

experiments below other than to calculate an approximate position to initiate the Kalman filter algorithm.

The measurement model used for an ionospheric-free phase measurement of a signal from a satellite s at receiver r, $\mathrm{h}_{\Phi_{\mathrm{IF},s}}$, is defined as follows:

$$\mathrm{h}_{\Phi_{\mathrm{IF},s}} = \rho_s + c\delta t_r + A_s + \mathrm{m}_G(\theta_s)T_{zwd} + \mathrm{m}_G(\theta_s)\cot\theta_s[G_N\cos\psi_s + G_E\sin\psi_s] \quad (1)$$

where ρ_s is the modeled geometric range between the receiver antenna reference point and the center of mass of satellite s in meters, c is the speed of light (299,792,458 m/s), δt_r is the receiver clock offset in seconds, A_s is the non-integer phase ambiguity of satellite s in meters, T_{zwd} is the zenith wet tropospheric delay in meters, m_G is the Global Mapping Function (GMF) (Boehm et al 2006) used to account for the increase in tropospheric delay when the satellite is not at the zenith, θ_s, ψ_s are receiver-satellite elevation and azimuth angles, respectively, G_N, G_E are the north and east troposphere gradients, respectively, and $\mathbf{x}$ is a vector of Kalman filter states that are to be estimated, i.e.

$$\mathbf{x} = (x_r \quad y_r \quad z_r \quad c\delta t_r \quad T_{zwd} \quad G_N \quad G_E \quad A_1 \quad ... \quad A_m)^{\mathrm{T}} \quad (2)$$

where x_r, y_r, z_r are the coordinates of the reference point of the receiver antenna and $A_1 ... A_m$ are the non-integer phase ambiguities, in meters, of m visible satellites. The hydrostatic (or 'dry') tropospheric delay has been removed using model UNB3 (Collins 1999). Other models applied include satellite and receiver antenna phase center offsets from the International GNSS Service (IGS), phase wind-up (Wu et al 1993), solid earth tides (IERS Conventions 2010), ocean tide loading (Lyard et al 2006) calculated by the Onsala Space Observatory (using Finite Element Solution FES2004 and the solid earth center as the reference frame origin) and polar tides (Kouba 2009) using data from the Center for Orbit Determination in Europe (CODE). Satellite coordinates and clock offsets from GPS system time are assumed to be known quantities because they are interpolated from precise 'final' satellite orbit and high-rate 5-second epoch rate clock files from the CODE. Of course, for a warning system, real-time clocks and orbits would have to be used. However, 'final' products are used here in order to show as fully as possible the effectiveness of the sidereal filter algorithms in removing high-frequency phase multipath errors.

The PPP algorithm used to estimate the coordinates of a receiver antenna is based upon a Kalman filter (Groves 2013) of which the system update equations are defined as:

$$\hat{\mathbf{x}}_k^- = \boldsymbol{\Phi}\hat{\mathbf{x}}_{k-1}^+ \quad (3)$$
$$\mathbf{P}_k^- = \boldsymbol{\Phi}\mathbf{P}_{k-1}^+\boldsymbol{\Phi}^{\mathrm{T}} + \mathbf{Q} \quad (4)$$

where $\hat{\mathbf{x}}_k^-$ is the time-propagated estimate of state vector at epoch k, $\hat{\mathbf{x}}_{k-1}^+$ is the estimate of the state vector at epoch $k-1$ following a measurement update, $\mathbf{P}_k^-$ is the time-propagated estimate of the error co-variance matrix at epoch k, $\mathbf{P}_{k-1}^+$ is the estimate of the error co-variance matrix at epoch $k-1$ following a measurement update and $\mathbf{Q}$ is the system noise co-variance matrix which is the same for every epoch.

This algorithm is designed to estimate the position of a static or near-static receiver, so the predicted state vector is always assumed to be identical to the estimated state

vector at the previous epoch, i.e. $\hat{\mathbf{x}}_k^- = \hat{\mathbf{x}}_{k-1}^+$. Hence, considering (3), the state transition matrix is simply the identity matrix: $\mathbf{\Phi} = \mathbf{I}$. Equation (4) also simplifies to $\mathbf{P}_k^- = \mathbf{P}_{k-1}^+ + \mathbf{Q}$.

The Kalman gain matrix $\mathbf{K}_k$ and the extended Kalman filter measurement update equations (Groves 2013) are defined as:

$$\mathbf{K}_k = \mathbf{P}_k^- \mathbf{H}_k^T \left(\mathbf{H}_k \mathbf{P}_k^- \mathbf{H}_k^T + \mathbf{R}_k \right)^{-1} \qquad (5)$$

$$\hat{\mathbf{x}}_k^+ = \hat{\mathbf{x}}_k^- + \mathbf{K}_k [\mathbf{z}_k - \mathrm{h}(\hat{\mathbf{x}}_k^-)] \qquad (6)$$

$$\mathbf{P}_k^+ = (\mathbf{I} - \mathbf{K}_k \mathbf{H}_k) \mathbf{P}_k^- \qquad (7)$$

where $\mathbf{P}_k^+$ is the estimate of the error covariance matrix at epoch k following a measurement update, $\mathbf{R}_k$ is the measurement noise covariance matrix at epoch k, $\hat{\mathbf{x}}_k^+$ is the estimate of the state vector at epoch k following a measurement update, $\mathbf{z}_k$ is a vector of measurements at epoch k and h is the vector of measurement functions of the state vector – one for each visible satellite – as defined in (1). $\mathbf{H}_k$ is the measurement matrix at epoch k where

$$\mathbf{H}_k = \left. \frac{\partial \mathrm{h}(\mathbf{x})}{\partial \mathbf{x}} \right|_{\mathbf{x} = \hat{\mathbf{x}}_k^-}$$

$$(8)$$

All ionospheric-free phase observations are assumed to have a standard deviation of $1/\sin\theta \times 0.015$ m, but satellites below an elevation angle of 10° are excluded.

The measurements from Day 1 are processed using this Kalman filter algorithm, but with the position states held fixed to the 'true' ECEF position of the receiver antenna and their respective standard deviations and noise power spectral densities (PSD) set to zero. For each epoch, the resulting ionospheric-free measurement residuals, defined as $\delta\mathbf{z}_k^+ = \mathbf{z}_k - \mathrm{h}(\hat{\mathbf{x}}_k^+)$, are time-tagged and stored in a database. The time series of phase residuals for each satellite are smoothed by a low-pass Butterworth filter with a cut-off frequency of 0.2 Hz. The purpose of this is to avoid the amplification of measurement noise when they are later applied as measurement corrections and yet preserve any short-period (5-20 s) multipath effects in those corrections. The resulting time series are *assumed* to largely represent the receiver-satellite range error caused by phase multipath interference although, of course, errors in the estimation of the state vector such as the receiver clock offset, troposphere delay and phase ambiguities will also alias into the residuals and hence the multipath corrections. They will also include those errors that have not been explicitly modeled such as higher-order ionospheric effects.

The measurements from Day 2 are then processed but with the position states no longer fixed. For each measurement z_τ at time τ, a correction for multipath error $\delta z_{\tau-T}$ from the database is applied that most closely corresponds with the epoch that preceded the measurement by approximately one sidereal period T. We use two methods to find a precise time shift:

1. One method is to choose a time shift that maximizes the dot-product of two receiver-to-satellite unit vectors associated with the current measurement and the potential correction that was derived from data gathered on the previous day. This approach is described in (Axelrad et al 2005) and is similar to the 'aspect repeat time'

method described in (Agnew and Larson 2007). This type of ODSF will hereafter be referred to as the 'dot-product' (DP) ODSF.

2. Another method is to calculate a repeat period using two values found in the GPS broadcast ephemeris for each satellite, specifically the square-root of the semi-major axis a_s and the correction to mean motion n_c, and Kepler's Third Law (Choi et al 2004). According to Agnew and Larson (2007), this repeat period T can be calculated as follows:

$$T = {4\pi}/{n} \quad \text{where} \quad n = \sqrt{GM}a_s^{-3} + n_c \qquad (9)$$

where GM is the standard gravitational parameter for earth, 3.986004×10^{14} m^{3}s^{-2}. This type of ODSF will hereafter be referred to as the 'broadcast ephemeris' (BE) ODSF.

A position-domain sidereal filter (PDSF) is also used. Measurements from Day 1 and Day 2 are processed separately by the PPP Kalman filter. The position error time series from Day 1 is smoothed using a low-pass Butterworth filter (0.2 Hz cut-off) to form time-tagged corrections. Each of these corrections is paired with a position solution from Day 2 using a time shift corresponding to the mean repeat period of all the satellites in view at that epoch. This period was relatively easy to calculate and could potentially be applied to real-time processing. Another method to determine the repeat time would be to choose one that produces the best correlation between the PPP position time series from the adjacent days over periods of a few hundred seconds (for example). Such a method would allow for the fact that not all signals at any one time are equally affected by multipath interference. However, this method is not applied here.

Overall performance
In order to assess the overall performance of each type of sidereal filter, each was applied to the data processing from two different continuously operating GPS receivers over an extended period of time during which conditions may be considered 'normal', i.e. a period of time was deliberately chosen where GPS measurements were free from satellite outages and no visible satellites had highly anomalous repeat periods. An analysis is made using data from the continuously operating GPS receivers named 'UEL' and 'UCL' operating at the University of East London and the University College London respectively. They form part of the Leica Geosystems 'SmartNet' real-time kinematic GPS network in the United Kingdom. These receivers have different antenna types and have contrasting surrounding environments. The overall performance of the sidereal filters is assessed by analyzing the resulting position time-series using Allan deviation as a performance measure.

For this trial, RINEX files from September 2 and 3, 2013 were used, each containing 24 hours of 1 Hz GPS code and phase measurements, with each dataset starting at midnight. Receiver UEL is equipped with a Leica AX1202GG ground plane antenna and, as can be seen in Figure 1, is sited close to a roof. In contrast, station UCL is equipped with a Leica AT504GG choke-ring antenna and sited in a more exposed rooftop location in an urban area and is *not* close to such a large single planar reflector. Reflected signals are more likely than at UEL to reach the antenna via horizontal 'far-field' reflectors such as surrounding buildings, causing shorter-period multipath errors (Larson et al 2007). For both receivers, all 24 hours of GPS phase

measurements from September 3 were processed using the PPP algorithm, as described in section 2, without applying any type of sidereal filter. Satellite pseudorandom noise code (PRN) 4 was excluded from all processing to ensure that satellite availability was the same on both days. The measurements were processed three more times: once with each type of ODSF and once with a PDSF applied as described above. An eight-hour period, 14:00 to 22:00, was chosen for analysis. This was the longest continuous period of time available for analysis for which the position time series was free of spurious signals originating from the precise clock data. For the sake of brevity, only the results from one position dimension, easting in the following case, are shown. The other components, northing and height, yield similar results and lead to the same conclusions.

Figure 2 shows the easting positioning errors over this time period. Notice firstly that station UEL exhibits more in the way of higher-frequency errors than station UCL. This is most likely to be because of where the UEL antenna is sited, as mentioned above, but may also be due in part to the design of the antenna at UEL being not as resistant to multipath interference as the choke-ring antenna at UCL. Hence, while the sidereal filters have generally been successful in removing the higher-frequency errors (i.e. with periods under about 1,000 s) at both stations, the effect is much more obvious at station UEL, where each of the time series associated with the sidereal filters appear much 'smoother' than those associated with standard PPP processing. This is understandable: a sidereal filter is likely to be more effective when acting on a dataset sourced from a receiver placed in a relatively high-multipath environment. Conversely, if GPS measurements have not been affected by strong multipath signals, then a sidereal filter will not yield a dramatic improvement.

Notice also that the PDSF has struggled to fully remove the higher-frequency positioning errors at station UEL between 18:00 and 19:30 whereas both of the ODSFs have had more success. This is because one of the satellites whose measurements are affected by strong phase multipath interference has a repeat time of 86,148 s. This differs significantly with the mean repeat time used by the PDSF of around 86,154 s. The ability of the sidereal filters in removing another example of high-frequency multipath error is examined later in this article.

Considering the eight-hour time period as a whole, the ODSFs have had a minimal impact on *accuracy* whereas the PDSF has at least improved the root-mean-square error (RMSE) of the UEL easting time series by 56%. Notice also that the performance of the ODSFs are nearly identical to each other. The poorer performance of the ODSFs in terms of accuracy is likely to be because the assumption that the Kalman filter residuals produced by standard PPP processing resembling multipath errors becomes less valid for lower-frequency multipath errors. These errors are more likely to be absorbed by slowly-varying Kalman filter states such as the wet troposphere zenith delay and the phase ambiguities and so are less likely to appear in the residuals, and it is these residuals that are used to form the multipath corrections for the ODSFs. Also, as the multipath corrections are being applied to the measurements, any low-frequency component of those corrections may also be absorbed by these slowly-varying Kalman filter states, which might explain why the ODSFs are not very effective at increasing stability in the position

time series over long time intervals. A PDSF on the other hand applies multipath corrections outside of the Kalman filter algorithm and so any low-frequency multipath corrections cannot alias into the Kalman filter states. However, all of the sidereal filters are noticeably more successful at increasing *stability* over much shorter time intervals, up to the order of a few minutes.

To quantify this increase in stability, Allan deviation is used (Allan 1966). Allan deviation has been used to analyze position time series in Dach et al (2009) and Friederichs (2010). It is a measure of signal stability across a time interval and can be used to identify different types of noise process (such as white or flicker noise and random walk) present in a signal. In this article, 'overlapping' Allan deviation is used rather than Allan deviation due to its superior performance over long averaging intervals. For a more comprehensive introduction to stability analysis using Allan deviation, the reader is recommended to refer to Riley (2008), Ferre-Pikal and Walls (2005) or Friederichs (2010).

Figure 3 shows the Allan deviation values across time intervals (τ-values) between 1 s and nearly 6,000 s (almost 1 hour and 40 minutes) corresponding to the eight-hour time series for UEL and UCL shown in Figure 2. When comparing these two figures, it is immediately clear that there is a difference between the impact that the sidereal filters have on the respective position error time series. It has already been noted that the standard PPP position solution from station UEL exhibits more in the way of higher-frequency positioning errors. Evidence for this can be seen in the black Allan deviation curve corresponding with standard PPP at UEL with the increase in gradient to positive values between time intervals of about 10 s and 40 s indicating that the dominant noise process over such time intervals cannot be considered stationary. In contrast, there is no such increase in Allan deviation for station UCL: the Allan deviation values for averaging intervals larger than about 10 s for standard PPP processing are all much lower than those at UEL, indicating that station UCL is less prone to multipath interference. However, all types of sidereal filter have successfully reduced Allan deviation values (i.e. increased the stability of the position time series) over intervals of between 10 s and about 900 s at UCL, albeit only slightly.

Nevertheless, in both cases, both types of ODSF have marginally outperformed the PDSF between time intervals of about 10 s and 1,000 s (about 17 minutes) as indicated by the lower Allan deviation values. Notice also that the gradient of the Allan deviation curves corresponding with the ODSFs are consistently close to -1 across all time intervals between about 10 s and 500 s, indicating that the dominant noise process in the position time series across time intervals of this size is close to white or flicker noise.

Notice also that both plots in Figure 3 indicate that the time series yielded by the ODSFs are less stable over time periods longer than about 1,000 s than that provided by the PDSF. As mentioned above, if the multipath corrections are applied at the observation level, the low-frequency component of those corrections are more likely to alias into the slowly-varying Kalman filter states such as the wet troposphere zenith delay and phase ambiguity states.

Figure 4 can be used to quantify the *improvement* in stability of the time series output by the ODSFs over those output by the PDSF. It shows the percentage improvement (i.e. percentage *reduction*) in Allan deviation given by the ODSFs relative to that resulting from the PDSF shown in Figure 3. Notice first of all that both of the ODSFs show an improvement in stability of over 5% for nearly all time intervals below about 200 s in length. However, the greatest improvement in stability differs between the two receivers. At UEL (Figure 4, top panel), the greatest improvement in stability of up to 16% occurs over time intervals of around 100 s whereas at UCL, a similar improvement occurs over much smaller intervals of around 10 s. Notice also that there does not seem to be much difference in performance at all between the two types of ODSF at UEL, but there is a slight advantage – no more than a couple of percentage points – to using a DP ODSF over a BE ODSF at UCL. UCL is more susceptible to short-period 'far-field' multipath interference. Of course, the repeat times calculated by the two methods are very similar to each other for each satellite. Indeed Figure 5, which is similar to a figure that appears in Larson et al (2007), shows that they agree to within just three seconds of each other for all satellites – an observation also made by Agnew and Larson (2007). However, from Figure 4 (bottom panel), it appears that these small differences have on average been influential in improving the performance of the DP ODSF, albeit only slightly.

So far, the analysis has focused on the 'average' performance of the sidereal filters over a long period of time. This would suggest that if a user is interested in analyzing relatively short time intervals of just a few minutes for monitoring purposes, then the use of an ODSF would be of greater benefit than a PDSF, although of course real-time satellite clock and orbits would have to be used. However, there are some important scenarios to consider if an ODSF is to be applied in this type of monitoring. One of these scenarios is the ability of the sidereal filters to remove the effect of strong high-frequency multipath where the choice of type of ODSF could be influential.

High-frequency multipath
The periodic positioning errors caused by multipath can be very similar to, for example, the movement caused by surface waves emanating from an earthquake epicenter (Larson et al 2007). A sidereal filter, unlike band-pass filtering for example, can in theory remove high-frequency positioning errors caused by multipath interference while leaving any true displacements intact.

Figure 6 (top panel) shows errors in northing resulting from different processing modes over a 15-minute period on March 27, 2012 at station UCL. For this particular receiver, this is a rare example of very-short period errors caused by multipath interference. This small part of a 24-hour position time series was chosen as an example of exceptionally high-frequency multipath error – in this case approximately 0.067 Hz (15-second period) most likely caused by a far-field reflector such as a tall building. It is conceivable, if this station alone was to be used for monitoring purposes, that the brief period of multipath error in the standard PPP time series could be misinterpreted as real movement. Both of the ODSFs are very successful at reducing the high-frequency multipath error and there seems to be little difference

between the two. This is confirmed by Figure 7 (top panel): all types of sidereal filter have been successful at reducing Allan deviation, i.e. increasing stability, over nearly all averaging intervals. However, the oscillatory pattern visible in the PDSF Allan deviation curve indicates that 15-second periodic multipath error, indicated by the first 'dip' in the curve, still remains while the curves for the two ODSFs have gradients close to -1 over all averaging intervals between 4 s and 80 s indicating that the position time series is dominated by white or flicker noise over these time intervals.

The above example showed the ODSF algorithms performing very well during a period of exceptionally high-frequency multipath. However, this is not always the case. Figure 6 (bottom panel) shows errors in easting resulting from different processing modes over another 15-minute period earlier on the same day. This time the sidereal filters do not seem to have made much of an improvement. In fact the PDSF has resulted in a worsening of stability. In contrast, the ODSFs have led to reduced Allan deviation values but clearly some of the periodic (approximately 22 s) multipath error remains. Note also that the BE ODSF outperforms the DP ODSF.

So why do the ODSFs perform so well between 23:05 and 23:20 but not so well between 18:20 and 18:35? An explanation perhaps lies in Figure 8. Here we see the smoothed ionospheric-free residuals for satellites G31 and G12 output from the PPP processing runs from five consecutive days (March 26–30, 2012) where the position states in the Kalman filter state vector have been fixed to their true values. It is the multipath interference affecting the phase measurements of the signals from these two satellites that cause the high-frequency multipath errors seen in Figure 6. These smoothed phase residuals have been color-coded by value and mapped onto a skyplot by azimuth and elevation. Notice that only very small 'patches' of sky are shown.

Notice the patterns formed by the color-coded residuals in Figure 8. Harris (2002) uses the term 'banding' to describe this pattern. In the case of satellite G31, it forms what appear to be parallel lines that are roughly orthogonal to the path or 'skytrack' taken by the satellite across the sky. Notice also that each skytrack is separated from the skytrack of an adjacent day by a very small angle of about 0.011°. Marked on this figure is the smoothed phase residual value for one particular epoch chosen as an example: 23:13:19 on March 27, 2012. Also marked is the location of the phase residual value found by both the DP ODSF and BE ODSF algorithms that is used as a correction. In this particular instance, both algorithms have chosen the same correction value, which means the aspect repeat time and the period calculated using elements from the broadcast ephemeris are identical.

Another example epoch is shown in the bottom panel of Figure 8 together with the respective corrections found by the two ODSF algorithms. Notice here that neither of the two corrections are optimal, although the value of the correction provided by the BE ODSF algorithm is a little more appropriate which would account for its slightly better performance exhibited in Figures 6 and 7 (lower panels). The reason for this is because the 'banding' pattern is not orthogonal to the path taken by satellite G12 across the sky. Therefore, the corrections found by the DP ODSF algorithm in

particular are out of phase with the error pattern of the 'current' day, and this is accentuated by the slightly larger angular separation between adjacent skytracks of 0.016°.

The bottom panel of Figure 8 also has implications for methods that use multiple days to form the sidereal multipath corrections, such as Langbein (2004) and Ragheb et al (2007) which use five and three days respectively. These studies use multiple days to form a mean correction (sometimes weighted) for multipath error to increase their robustness. However, again, the effectiveness of this method to remove high-frequency multipath depends on the distribution of the error due to multipath by satellite elevation and azimuth such as the 'banding' patterns seen above. If the angle that the satellite skytrack makes with the lines formed by a banding pattern is clearly not orthogonal, then any method that uses multiple days must take this into account. Otherwise, the ability of such a sidereal filter to remove high-frequency multipath error will be reduced further.

One solution to this problem posed by high-frequency multipath is to do away with the need to calculate a repeat time altogether and adopt a method that maps measurement residuals onto a hemisphere by azimuth and elevation to form a hemispherical template of multipath corrections. Studies such as Wanninger and May (2000) and Harris (2002) right through to Fuhrmann et al (2014) and Moore et al (2014) have all mapped residuals by azimuth and elevation. However, most of these have stacked the residuals into cells of varying sizes, for example 1° × 1° in azimuth and elevation (Bilich and Larson 2008). These usually aim to capture the slowly oscillating multipath effect that often affects measurements from satellites at low elevation angles. However, even a cell size of 0.5° × 0.5° clearly will not capture high-frequency multipath effects such as those illustrated in Figure 8. Importantly, even lower-frequency multipath effects with a period of a few hundred seconds will be lost if such cell sizes are used. If the motivation is to reduce high-frequency multipath error, then one potential solution would be to process historical measurement data to produce a hemispherical scatter plot of individual measurement residuals, as presented in Figure 8, and then interpolate or extrapolate a correction for a particular azimuth and elevation as necessary. The author has not yet explored this. Nevertheless, stacking measurement residuals into cells as described is not suited to reducing high-frequency multipath error.

Conclusions and discussion
It can be seen from each of the examples above that the observation-domain sidereal filters (ODSFs) produce a more stable position time series than a position-domain sidereal filter (PDSF) over time intervals of under about 1,000 s. Certainly, for nearly all time intervals under about 200 s, the time series output from the PPP algorithm after the application of a ODSF is 5-16% more stable, in terms of Allan deviation, than those output after applying a PDSF. For longer averaging intervals, the converse is true in these particular cases. This is likely to be due to the fact that if corrections are applied at the observation level, their low-frequency components are likely to be absorbed into the slowly-varying states such as the zenith wet tropospheric delay, thus illustrating a significant limitation of the ODSF algorithm. Despite this, it is likely to be of some benefit to earthquake and tsunami early

warning systems since these require the accurate but prompt measurement of potentially small ground displacements.

However, the ODSFs, although they have been shown to outperform a PDSF here, are not a panacea. During periods of high-frequency multipath, even the ODSFs may struggle to remove the effect of multipath. This is not because of an inability to calculate an accurate satellite repeat time, but because of the complicated nature of the multipath itself and the fact that the path that a satellite takes across the sky is not exactly the same from one day to the next. Indeed, the intricate patterns that multipath errors form when mapped by azimuth and elevation, such as those in Figure 8, can be highly influential in determining how effective the ODSFs are. So despite the application of such a filter, the risk would remain that errors due to multipath interference could still be misinterpreted as surface waves emanating from an earthquake epicenter and vice versa. Also, there is little difference between the two methods used here to calculate these repeat times: aspect repeat time and repeat times calculated using the broadcast ephemeris. If there is any difference in performance between the two types of ODSF, it is because of the complicated nature of the multipath error itself and not that one method is necessarily better than the other.

These intricate patterns also have consequences for other methods of phase multipath mitigation not applied in this study. Methods that use multiple days to form the multipath corrections can potentially lose the ability to correct for high-frequency multipath, no matter how well the repeat times of satellites are calculated. Other methods stack phase multipath residuals into 'cells' of certain sizes in terms of azimuth and elevation and an average value is calculated for each. These cell sizes, even those of 0.5° × 0.5°, are too large to capture any patterns formed by high-frequency multipath errors.

Author biographies
Christopher Atkins is a PhD candidate at University College London. He is currently working to improve GNSS precise point positioning for tsunami early warning systems. He received his MSc in Geodetic Surveying with distinction from the University of Nottingham in 2006.

Marek Ziebart is a Professor of Space Geodesy at University College London. His research interests include spacecraft orbit determination and prediction, photon pressure modeling for space vehicles, high precision processing of GPS data, the definition of planet scale reference frames and surfaces and the design and

simulation of system architecture of navigation and positioning systems for other planets.

Figures

Fig. 1 Antennas of continuously operating GPS receivers at UEL (top) and UCL (bottom) that were used in the experiment. These stations are part of the Leica Geosystems 'SmartNet' real-time kinematic GPS network in the United Kingdom. Photograph used with permission from Leica Geosystems.
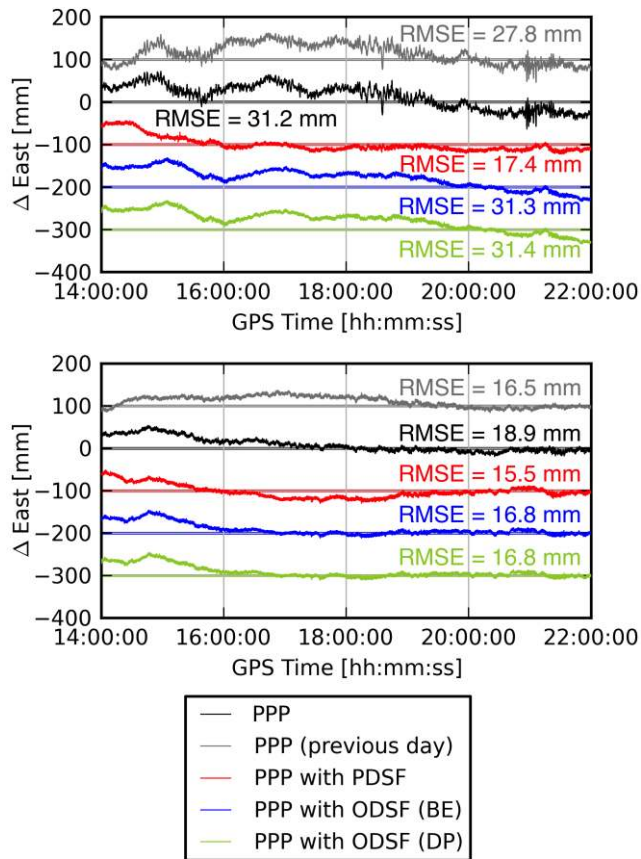
Fig. 2 Easting position errors between 14:00 and 22:00 on September 3, 2013 for stations UEL (top) and UCL (bottom) resulting from standard PPP processing and PPP processing with various types of sidereal filter applied. The root-mean-square error (RMSE) of each time series is shown. Each of the time series have been offset from each other by appropriate multiples of 100 mm for clarity.
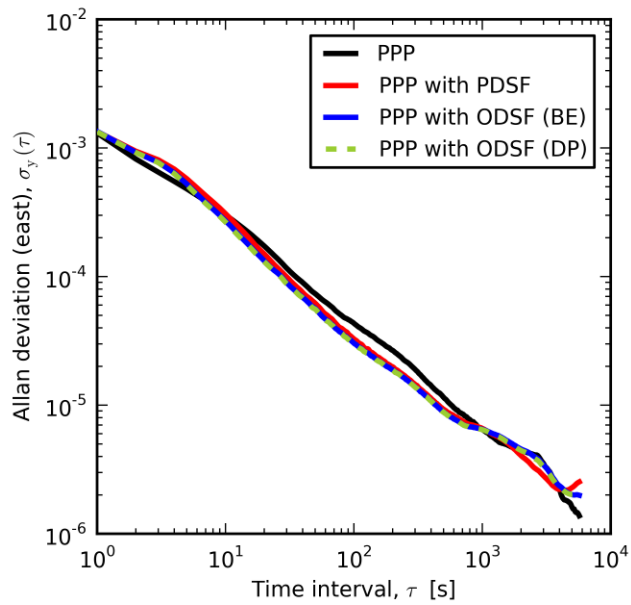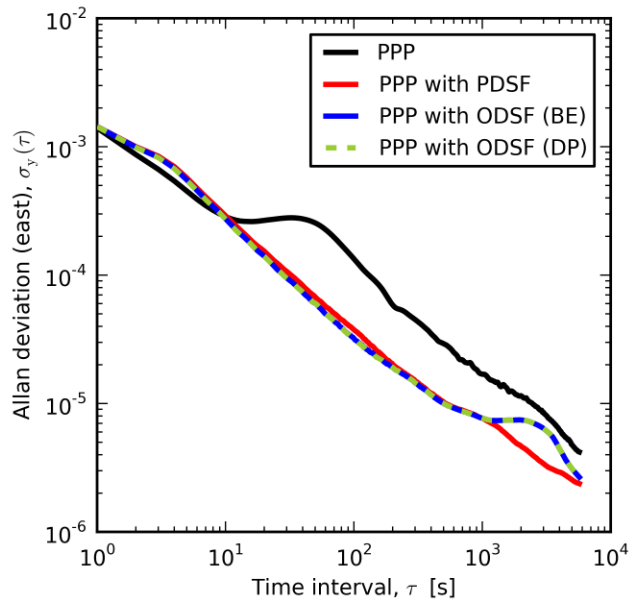
Fig. 3 Allan deviation plots of the easting position time-series at stations UEL (top) and UCL (bottom) between 14:00 and 22:00 on September 3, 2013 shown in Figure 2.
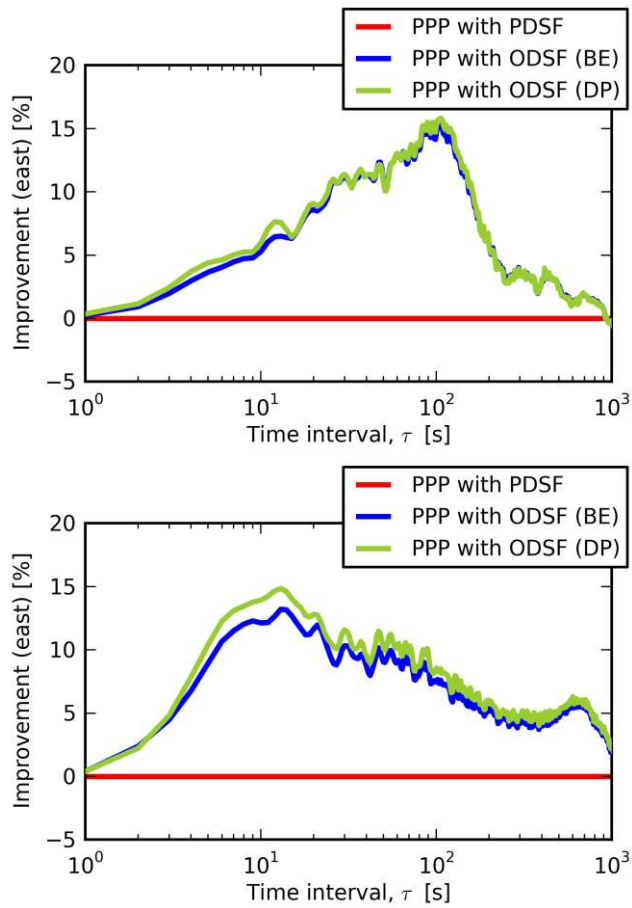
Fig. 4 The percentage improvement (i.e. reduction) in Allan deviation values shown in Figure 3 as a result of applying an ODSF relative to applying a PDSF: Stations UEL (top) and UCL (bottom).
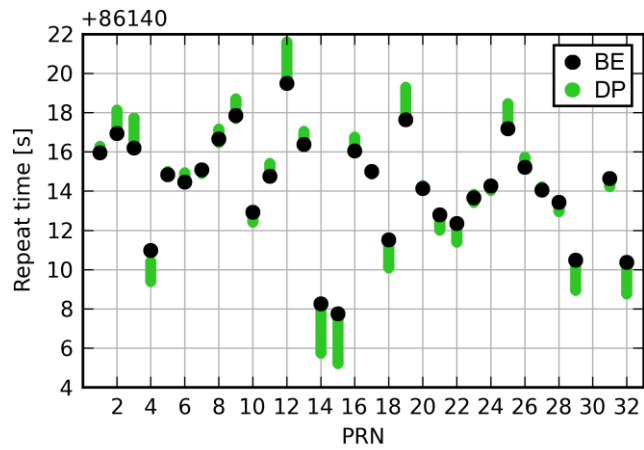
Fig. 5 Orbit repeat times calculated using elements in the broadcast ephemeris (BE) and the ranges of repeat times calculated by the DP method for each GPS satellite PRN tracked at UCL on September 3, 2013.
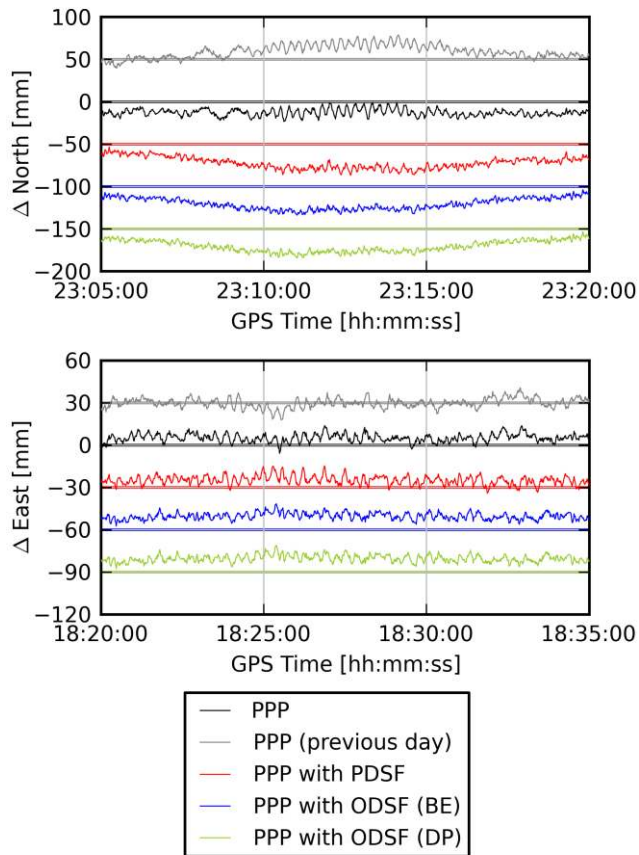
Fig. 6 Position errors on March 27, 2012, 23:05 – 23:20 (top), 18:20 – 18:35 (bottom) for station UCL resulting from standard PPP processing and PPP processing with various types of sidereal filter applied. (Each of the time series have been offset from each other by appropriate multiples of 50 mm or 30 mm for clarity).
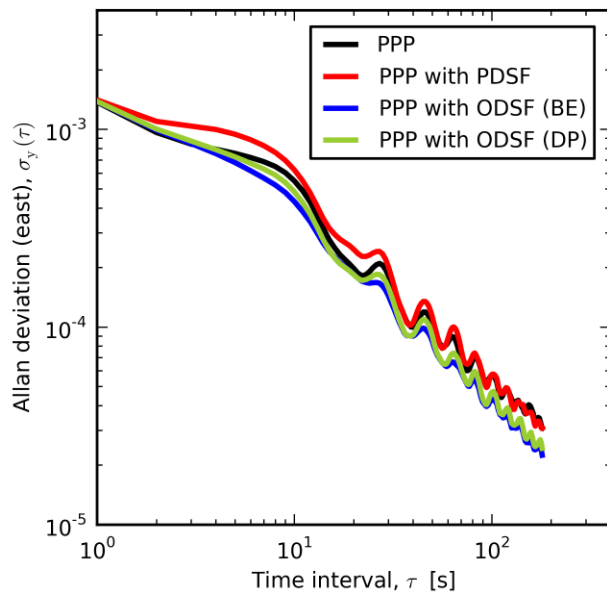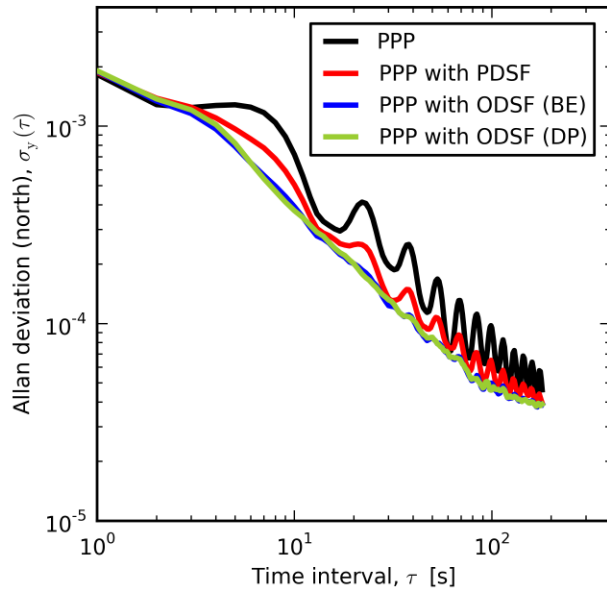
Fig. 7 Allan deviation plots of position time-series for station UCL on March 27, 2012 shown in Figure 6: 23:05 – 23:20 (top), 18:20 – 18:35 (bottom)
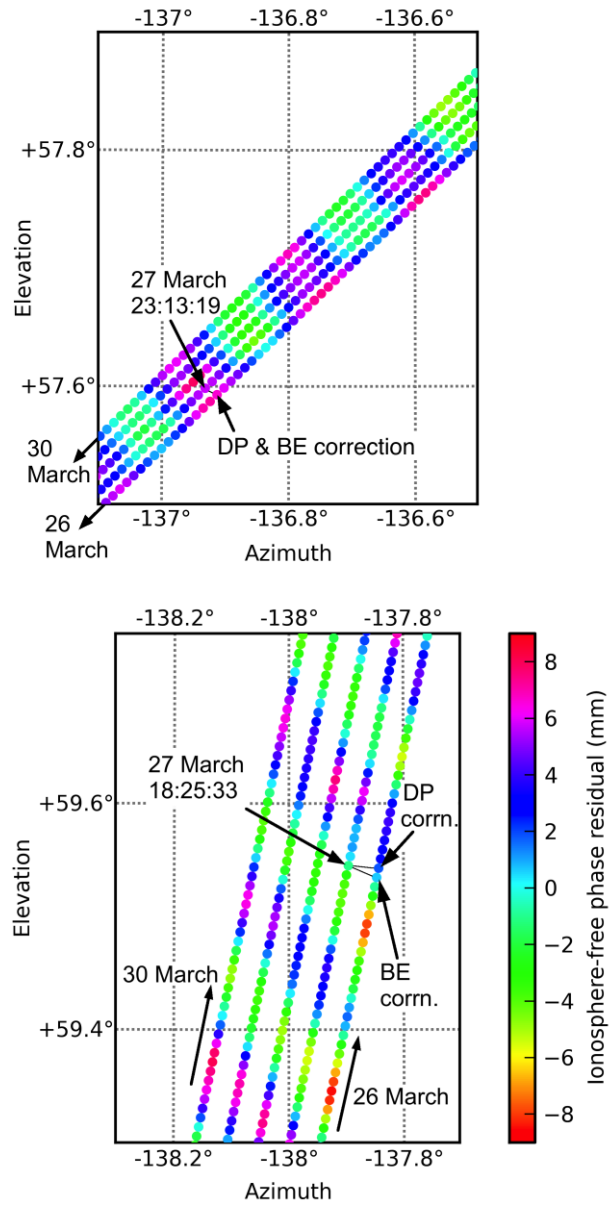
Fig. 8 Two skyplots of smoothed ionospheric-free phase measurement residuals associated with satellites G31 (top) and G12 (bottom) on March 26-30, 2012. ('corrn.' – 'correction')

References

Agnew DC, Larson KM (2007) Finding the repeat times of the GPS constellation. GPS Solut 11:71–76. doi: 10.1007/s10291-006-0038-4

Allan DW (1966) Statistics of atomic frequency standards. Proc IEEE 54:221–230. doi: 10.1109/PROC.1966.4634

Axelrad P, Larson KM, Jones B (2005) Use of the correct satellite repeat period to characterize and reduce site-specific multipath errors. Proc. ION GNSS 2005, Inst. Navig. Long Beach, CA, pp 2638–2648

Bilich A, Larson KM (2008) Mapping the GPS multipath environment using the signal-to-noise ratio (SNR). Radio Sci 42:RS6003. doi: 10.1029/2007RS003652

Bilich AL, Cassidy JF, Larson KM (2008) GPS seismology: Application to the 2002 Mw 7.9 Denali Fault earthquake. Bull Seismol Soc Am 98:593–606. doi: 10.1785/0120070096

Bock Y (1991) Continuous monitoring of crustal deformation. GPS World 2:40–47.

Boehm J, Niell A, Tregoning P, Schuh H (2006) Global Mapping Function (GMF): A new empirical mapping function based on numerical weather model data. Geophys Res Lett 33:L07304. doi: 10.1029/2005GL025546

Choi K, Bilich AL, Larson KM, Axelrad P (2004) Modified sidereal filtering: Implications for high-rate GPS positioning. Geophys Res Lett 31:L22608. doi: 10.1029/2004GL021621

Collins JP (1999) Assessment and development of a tropospheric delay model for aircraft users of the global positioning system. Dissertation. University of New Brunswick

Dach R, Brockmann E, Schaer S, et al (2009) GNSS processing at CODE: status report. J Geod 83:353–365. doi: 10.1007/s00190-008-0281-2

Elósegui P, Davis JL, Oberlander D, et al (2006) Accuracy of high-rate GPS for seismology. Geophys Res Lett 33:L11308. doi: 10.1029/2006GL026065

Ferre-Pikal ES, Walls FL (2005) Frequency standards, characterization. Encycl RF Microw Eng. doi: 10.1002/0471654507

Friederichs T (2010) Analysis of geodetic time series using Allan variances. Dissertation. University of Stuttgart

Fuhrmann T, Luo X, Knöpfler A, Mayer M (2014) Generating statistically robust multipath stacking maps using congruent cells. GPS Solut 19:83–92. doi: 10.1007/s10291-014-0367-7

Geng J, Bock Y, Melgar D, et al (2013) A new seismogeodetic approach applied to GPS and accelerometer observations of the 2012 Brawley seismic swarm: Implications for earthquake early warning. Geochemistry, Geophys Geosystems 14. doi: 10.1002/ggge.20144

Genrich JF, Bock Y (1992) Rapid resolution of crustal motion at short ranges with the global positioning system. J Geophys Res 97:3261–3269. doi: 10.1029/91JB02997

Granström C, Site-dependent effects in high-accuracy applications of GNSS. Technical Report. Chalmers University of Technology

Groves PD (2013) Principles of GNSS, Inertial, and Multisensor Integrated Navigation Systems, 2nd edn. Artech House, London

Harris RB (2002) Evaluation, refinement and fusion of software-based pseudorange multipath mitigation techniques. Proc. ION GPS 2002, Inst. Navig. Portland, OR, pp 460–471

Hung H-K, Rau R-J (2013) Surface waves of the 2011 Tohoku earthquake: Observations of Taiwan's dense high-rate GPS network. J Geophys Res Solid Earth 118:332–345. doi: 10.1029/2012JB009689

IERS Conventions (2010), Petit G and Luzum B (eds.) (IERS Technical Note 36) Frankfurt am Main: Verlag des Bundesamts für Kartographie und Geodäsie, 2010.

Kouba J (2009) A guide to using International GNSS Service (IGS) products. https://igscb.jpl.nasa.gov/igscb/resource/pubs/UsingIGSProductsVer21.pdf. Accessed 16 June 2015

Langbein J (2004) High-rate real-time GPS network at Parkfield: Utility for detecting fault slip and seismic displacements. Geophys Res Lett 13:L15S20. doi: 10.1029/2003GL019408

Larson KM, Bilich A, Axelrad P (2007) Improving the precision of high-rate GPS. J Geophys Res Solid Earth 112:B05422. doi: 10.1029/2006JB004367

Lau L (2012) Comparison of measurement and position domain multipath filtering techniques with the repeatable GPS orbits for static antennas. Surv Rev 44:9–16. doi: 10.1179/1752270611Y.0000000003

Leick A, Rapoport L, Tatarnikov D (2015) GPS Satellite Surveying, 4th edn. John Wiley & Sons, Inc., Hoboken, NJ

Lyard F, Lefevre F, Letellier T, Francis O (2006) Modelling the global ocean tides: Modern insights from FES2004. Ocean Dyn 56:394–415. doi: 10.1007/s10236-006-0086-x

Misra P, Enge P (2001) Global Positioning System: Signals, Measurements, and Performance, 1st edn. Ganga-Jamuna Pr, Lincoln, Mass.

Moore M, Watson CS, King MA, et al (2014) Empirical modelling of site-specific errors in continuous GPS data. J Geod 88:887–900. doi: 10.1007/s00190-014-0729-5

Ragheb AE, Clarke PJ, Edwards SJ (2007) GPS sidereal filtering: coordinate- and carrier-phase-level strategies. J Geod 81:325–335. doi: 10.1007/s00190-006-0113-1

Reuveni Y, Kedar S, Owen SE, et al (2012) Improving sub-daily strain estimates using GPS measurements. Geophys Res Lett 39:L11311. doi: 10.1029/2012GL051927

Riley WJ (2008) Handbook of frequency stability analysis. National Institute of Standards and Technology. Boulder, Colo

Shi J (2012) Precise Point Positioning Integer Ambiguity Resolution with Decoupled Clocks. Thesis. University of Calgary

Takasu T (2006) High-rate precise point positioning: observation of crustal deformation by using 1-Hz GPS data. GPS/GNSS Symp. 2006, Tokyo.

Wanninger L, May M (2000) Carrier phase multipath calibration of GPS reference stations. Proc ION GPS 2000, Inst Navig. Salt Lake City, UT, pp 113–124.

Wu JT, Wu SC, Hajj GA, et al (1993) Effects of Antenna Orientation on GPS Carrier Phase Measurements. Manuscripta Geod 18:91–98.

Zumberge JF, Heflin MB, Jefferson DC, et al (1997) Precise point positioning for the efficient and robust analysis of GPS data from large networks. J Geophys Res 102:5005–5017.